DOI: 10.1002/ejic.201100384

Anchoring of Ru–Pt and Ru–Au Clusters onto a Phosphane-Functionalized Carbon Support

Christopher Willocq,[a] Deborah Vidick,[a] Bernard Tinant,[a] Arnaud Delcorte,[b] Patrick Bertrand,[b] Michel Devillers,[a] and Sophie Hermans*[a]

Keywords: Nanoparticles / Cluster compounds / Ruthenium / Carbon support

Two mixed-metal clusters, $[Ru_5PtC(CO)_{14}(COD)]$ (**1**) and $[Ru_6Au_2C(CO)_{16}(PPh_3)_2]$ (**2**), were anchored onto a prefunctionalized active carbon support (C_{PPh_2}) with chelating phosphane groups on its surface. These clusters were also deposited onto the unmodified support (C_{SX+}) for comparison. The incorporation of **1** and **2** on both supports was studied by a combination of SIMS and XPS. When the clusters were anchored onto the functionalized carbon support, SIMS spectra displayed characteristic patterns that were different from those obtained in the case of their deposition on the unmodified support. In the latter case, spectra corresponded to the results obtained with pure unsupported clusters. XPS analyses of the supported species seemed to indicate that the stoichiometry of the clusters was retained after anchoring and that their dispersion was better on C_{PPh_2} than on C_{SX+}. This indicates that the phosphanes act as anchors for noble metal compounds through a ligand exchange mechanism. The supported samples were then thermally activated and characterized by SIMS, XPS, TEM/EDXS and XRD. Analyses by SIMS showed that the cluster ligand shell was removed during thermal treatment. XPS measurements indicated that the composition of the supported particles corresponded to that of the starting clusters and that the dispersion remained higher in the case of C_{PPh_2}. Well-dispersed bimetallic-supported nanoparticles (1–2 nm) were obtained when cluster **1** was used as the precursor, whereas anchoring of cluster **2** resulted in its fragmentation leading to supported nanoparticles of variable stoichiometries. Reactions with soluble model molecules were carried out to prove the chemical bonding of **1**. Crystallization of the new cluster $[Ru_5PtC(CO)_{14}\{(PPh_2CH_2)_2NC_3H_7\}]$ confirmed the chemical bonding of cluster **1** onto the C_{PPh_2} support through a ligand exchange mechanism involving COD.

Introduction

Because of their molecular nature and solubility in most organic solvents, metal clusters have been claimed for a long to be suitable precursors for the preparation of nanoparticles with a well-defined size and stoichiometry.[1] When supported nanoparticles are to be used for applications in heterogeneous catalysis for instance,[2–4] close attention has to be paid to the cluster-surface interaction. In particular, many questions arise as to the relationship between the cluster nuclearity and the final particle size, because most of the time surface diffusion and agglomeration can not be totally avoided. Clusters have already been chemically grafted onto solid supports like polymer beads or dendrimers[5,6] but, as far as we know, never onto active carbon, which is an appropriate support for many practical uses, namely catalytic processes in an aqueous phase. Some examples of molecular clusters deposited onto active carbon, without any particular interaction with the support, were developed to prepare supported catalysts for hydrogenation or ammonia synthesis.[7–9] Active carbon supports have been chemically functionalized with amines for example,[10] in order to prepare catalysts for epoxidation or aziridination reactions,[11,12] or to immobilize chiral complexes for enantioselective catalysis.[13] Given the nonbulk behaviour of nanometer-sized particles, it is important to understand the structure–activity relationship of supported nanoparticles. Nuzzo et al. have carried out some studies to characterize in detail the structure of supported Ru–Pt nanoparticles prepared by deposition of heteronuclear Ru–Pt clusters on carbon black.[14–17] Even by using clusters as precursors, the supported samples presented a particle size distribution, from which it follows that clusters need to be anchored onto the surface to avoid agglomeration. The development of carbon-supported cluster-derived nanoparticles is a challenge because obtaining a control at the nanoscopic level of the surface chemistry of carbon supports has seldom been achieved because of the difficulty in characterizing the samples spectroscopically. The potentiality of organometallic and coordination chemistry as tools to devise a

[a] Institut de la Matière Condensée et des Nanosciences (IMCN/MOST), Université Catholique de Louvain,
Place Louis Pasteur 1/3, 1348 Louvain-la-Neuve, Belgium
Fax: +32-10-472330
E-mail: Sophie.Hermans@uclouvain.be
[b] Institut de la Matière Condensée et des Nanosciences (IMCN/BSMA), Université Catholique de Louvain,
Croix du Sud 1, 1348 Louvain-la-Neuve, Belgium
Supporting information for this article is available on the WWW under http://dx.doi.org/10.1002/ejic.201100384.

molecular strategy able to favour covalent interaction between cluster and carbonaceous supports has so far been underemployed. After thermal treatment, the clusters should give the desired carbon-supported nanoparticles. Moreover, it is possible to study the anchoring mechanism in solution, by using soluble mimics of the surface ligands.

Here, we report on the anchoring of two heterometallic clusters, $[Ru_5PtC(CO)_{14}(COD)]$ (COD = cyclooctadiene) (**1**) and $[Ru_6Au_2C(CO)_{16}(PPh_3)_2]$ (**2**), onto an active carbon support specifically functionalized for that purpose (C_{PPh_2}).[18] This active carbon with a high specific surface area was treated in order to introduce chelating phosphane groups onto its surface. Secondary ion mass spectrometry (SIMS), in combination with XPS, TEM/EDXS and XRD, enabled us to characterize the fate of these mixed-metal clusters at each step of the synthesis and thermal treatment. This provides unique and powerful monitoring at the molecular level of the anchoring and activation processes occurring at the surface of the carbon support. The supported clusters were subsequently thermally treated to yield supported nanoparticles. To better understand the anchoring mechanism, model reactions in solution were carried out. The $(PPh_2CH_2)_2NC_3H_7$ ligand, which closely mimics the functions present at the surface of C_{PPh_2}, was synthesized and its reaction with cluster **1** and **2** was studied.

Results and Discussion

1. Anchoring and Activation

Cluster **1** was prepared as described previously[19] from $(PPN)_2[Ru_5C(CO)_{14}]$ [PPN = bis(triphenylphosphoranylidene)ammonium] and $[Pt(COD)Cl_2]$. Cluster **2**, which is also known,[20] was prepared here by a new, easier route from $(PPN)_2[Ru_6C(CO)_{16}]$ and $Au(PPh_3)Cl$. Both clusters (Scheme 1) were unambiguously identified by their IR spectra. A phosphane-functionalized support noted as C_{PPh_2}[18] (Scheme 1) was prepared in several steps from SXplus-activated carbon (noted as C_{SX+}, Norit). First, the number of oxygenated surface groups was increased by HNO_3 oxidation and quantified by Boehm's titrations and XPS.[21] Then, the carboxylic acid groups were treated with $SOCl_2$ to transform them into acyl chlorides, before coupling them with ethylenediamine. The pendant amine functions were finally derivatized into chelating phosphanes by the concomitant action of $HPPh_2$ and CH_2O.[18] XPS characterization of the final C_{PPh_2} support revealed a P/C surface ratio of ca. 0.01, corresponding to about 2.5 anchoring sites (chelating phosphanes) per nm^2, which is a very high density of functional groups. When C_{PPh_2} was submitted to thermogravimetric analysis (TGA) under nitrogen, it displayed a three-step weight loss of 3% below 250 °C, 21% between 250 and 450 °C and 20% between 450 and 900 °C. This can be attributed to the stepwise decomposition of the grafted functions when heated. It shows that the functions are indeed firmly bound to the surface as otherwise (in the case of a mere physical mixture) much lower decomposition temperatures would be observed.

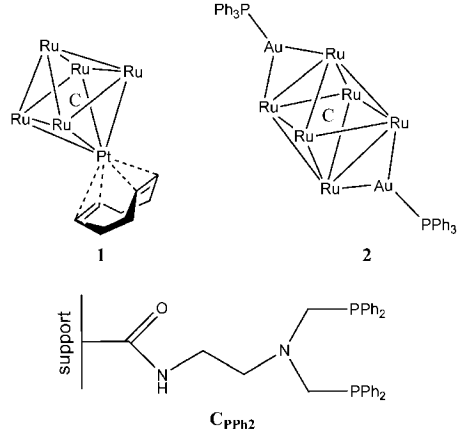

Scheme 1. Cluster **1**, **2** and the functionalized carbon support C_{PPh_2}. Carbonyl ligands in clusters **1** and **2** are omitted for clarity.

The two clusters **1** and **2** were anchored onto the phosphane-functionalized support C_{PPh_2} by stirring in a mixture of solvents, and deposited onto the unmodified carbon support (C_{SX+}) for comparison. The total metal loading (determined by Ru atomic absorption analysis of the filtrates) after incorporation on C_{PPh_2} was 7.8 and 4.2 wt.-% for **1** and **2**, respectively, and was 10 wt.-% for both on C_{SX+}.

The obtained solid samples were characterized by secondary ion mass spectrometry (SIMS) and X-ray photoelectron spectroscopy (XPS). The SIMS spectra obtained for cluster **1** are displayed in Figure 1. In the case of the pure unsupported cluster (Figure 1, a) the high-mass region consists of several peaks corresponding to the loss of ligands, which is a typical fragmentation pattern for clusters. Considering that the SIMS spectrum of cluster **1** deposited onto C_{SX+} (Figure 1, b) is the same as the reference spectrum for the pure, unsupported cluster (Figure 1, a), and that the experimental Ru/Pt surface atomic ratio obtained by XPS (Table 1 and Annex 2, see Supporting Information) corresponds to the stoichiometry of the cluster, one can conclude that cluster **1** was incorporated onto C_{SX+} in a molecularly intact fashion.[22] The SIMS spectrum of cluster **1** anchored onto C_{PPh_2} is different (Figure 1, c): the highest mass peak observed at m/z = 1287 is attributed to the fragment $[Ru_5PtC(CO)_{14}(PPh_2)]^-$. The PPh_2 ligand in this species originates from the phosphane groups of the functionalized support, proving that a chemical reaction occurred as expected between the support and the cluster. Moreover, it is known that the COD ligand in this cluster is readily exchanged for chelating phosphanes.[23] As the COD ligand was not observed anymore in the SIMS spectrum, it can be speculated that cluster **1** is attached onto C_{PPh_2} by a ligand exchange mechanism as illustrated in Scheme 2. The SIMS spectrum of the anchored cluster also comprises successive fragments corresponding to CO losses {down to m/z = 1012, $[Ru_5PtC(CO)_4(PPh_2)]^-$}, a further phenyl loss {m/z = 933, $[Ru_5PtC(CO)_4(PPh)]^-$}, and so on, finally leaving the naked metallic core (m/z = 713, $[Ru_5PtC]^-$). The Ru/Pt atomic surface ratio determined by XPS for cluster **1** anchored onto C_{PPh_2} is also similar to the calculated value (see

Table 1 and Annex 2), indicating that the cluster stoichiometry is essentially retained after anchoring. Moreover, the M/C ratios (M = Ru or Pt) are higher on C_{PPh_2} than on C_{SX+}, suggesting a higher surface concentration (i.e. better spreading) when the cluster is anchored rather than deposited.

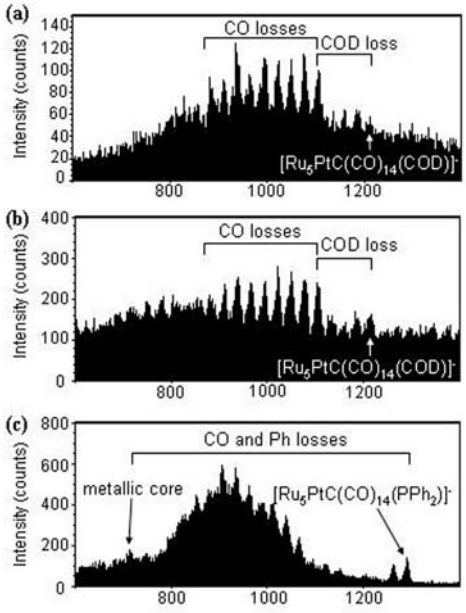

Figure 1. Negative SIMS spectra of the cluster $[Ru_5PtC(CO)_{14}(COD)]$ (**1**) before thermal treatment: (a) pure unsupported cluster as reference, (b) cluster **1** deposited onto C_{SX+} and (c) cluster **1** anchored onto C_{PPh_2}.

Table 1. XPS results for cluster **1**.

Ratio	Before thermal treatment				After thermal treatment			
	C_{SX+} Calcd.[a]	Exp.	C_{PPh_2} Calcd.[a]	Exp.	C_{SX+} Calcd.[a]	Exp.	C_{PPh_2} Calcd.[a]	Exp.
Ru/Pt	5	4.81	5	4.33	5	4.66	5	4.20
Ru/C	0.009	0.015	0.007	0.027	0.009	0.011	0.007	0.022
Pt/C	0.002	0.003	0.001	0.006	0.002	0.002	0.001	0.005

[a] The calculated values are bulk molar ratios. Before thermal treatment the amount of C taken into consideration for the calculations corresponds to the sum arising from the carbon support, the carbonyl ligands and the central carbide atom of the clusters. After heating the amount of C considered results only from the carbon support and the central carbide atom of the clusters.

The SIMS spectra obtained for cluster **2** are displayed in Figure 2. The SIMS spectrum of **2** deposited onto C_{SX+} (Figure 2, b) is similar to that of the pure unsupported cluster (Figure 2, a). The peak with the highest *m*/*z* value is observed at *m*/*z* = 1405 $\{[Ru_6Au_2C(CO)_{14}]^-\}$, and is followed by a series of peaks corresponding to CO losses down to *m*/*z* = 1154 $\{[Ru_6Au_2C(CO)_5]^-\}$. The experimental Ru/Au surface atomic ratio obtained by XPS for this sample corresponds to the stoichiometry of the cluster (Table 2 and Annex 2). This indicates that cluster **2** was also molecularly intact when deposited onto C_{SX+}. When cluster **2** was anchored onto C_{PPh_2} (Figure 2, c), a similar fragmentation pattern was observed by SIMS but with a shift of *m*/*z* =

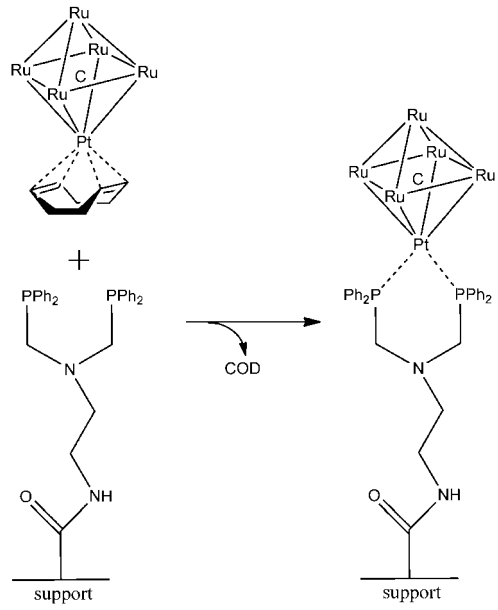

Scheme 2. Anchoring model for cluster **1** on C_{PPh_2}. Carbonyl ligands are omitted for clarity.

197, which corresponds to one gold atom. The highest mass peak is observed at *m*/*z* = 1235 $\{[Ru_6AuC(CO)_{15}]^-\}$ followed by fragments corresponding to CO losses {down to *m*/*z* = 957, $[Ru_6AuC(CO)_5]^-$}. Once more, the difference in SIMS spectra for **2** on C_{SX+} or C_{PPh_2} indicates that a chemical reaction occurred between the functionalized support and the cluster. However, there is no observable peak attributable to the entire Ru_6Au_2 metallic core anymore. It is therefore necessary to determine whether the cluster breaks

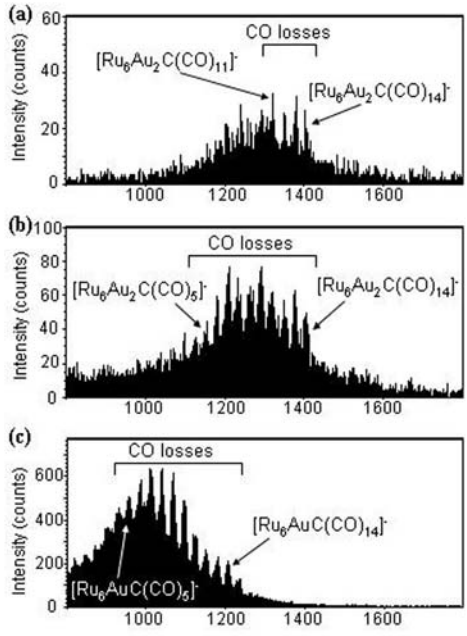

Figure 2. Negative SIMS spectra of the cluster $[Ru_6Au_2C(CO)_{12}(PPh_3)_2]$ (**2**) before thermal treatment: (a) pure unsupported cluster as reference, (b) cluster **2** deposited onto C_{SX+} and (c) cluster **2** anchored onto C_{PPh_2}.

down during anchoring or during the SIMS analyses. The Ru/Au atomic surface ratio for cluster **2** on C_{PPh_2} (Table 2) corresponds also to the global composition of the starting cluster, which does not mean that both metals did not segregate at the microscopic scale after incorporation onto the support. The M/C ratios (M = Ru and Au) are higher in the case of the functionalized support, showing again that the cluster surface distribution is probably better on C_{PPh_2} than on C_{SX+}.

Table 2. XPS results for cluster **2**.

Ratio	Before thermal treatment				After thermal treatment	
	C_{SX+}		C_{PPh_2}		C_{PPh_2}	
	Calcd.[a]	Exp.	Calcd.[a]	Exp.	Calcd.[a]	Exp.
Ru/Au	3	3.09	3	2.74	3	2.88
Ru/C	0.007	0.008	0.003	0.019	0.003	0.009
Au/C	0.002	0.003	0.001	0.007	0.001	0.003

[a] See Table 1.

These supported clusters were treated thermally (experimental conditions determined after TGA analyses, see Table 3) in order to prepare supported nanoparticles by removing the ligand shell. The activated samples were analyzed by SIMS, XPS, TEM and XRD. After thermal treatment, the high-mass peaks disappear from the SIMS spectra on both supports, indicating that all the ligands were actually removed. Nevertheless, the low-mass region still displays the typical isotopic patterns of ruthenium and platinum for **1** and of ruthenium and gold for **2** (Annex 1, see Supporting Information) showing the presence of the desired metals at the surface. The XPS results (see Tables 1 and 2 and Annex 2 in the Supporting Information) show a slight change in the Ru/Pt and Ru/Au ratios, indicating that some modification of the cluster structure occurred during thermal treatment. In all cases, the M/C ratios obtained after thermal treatment were smaller than before, suggesting a possible agglomeration of the clusters during heating. Nevertheless, the M/C ratios remained higher on C_{PPh_2} even after activation. After thermal treatment, TEM images of cluster **1** supported on C_{PPh_2} show that homogeneously dispersed nanoparticles 1–2 nm in size were obtained (Figure 3, a). These small sizes were confirmed from XRD analyses by the absence of any peak in the X-ray diffractogram [Annex 4 (Supporting Information)]. In the case of cluster **2** on C_{PPh_2}, TEM images show that well-dispersed nanoparticles (1–2 nm) are also obtained (Figure 3, b), but with the concomitant presence of bigger particles (10–20 nm) (Figure 3, c). For this sample, the X-ray diffractogram presents peaks corresponding to metallic gold indicating the presence of gold crystallites at the surface (see Annex 4, Supporting Information). We infer that, as in the case of cluster **1**, the smallest particles containing Ru are too small to give any XRD signal, while Au is present in the form of bigger particles that give rise to a diffraction pattern. The EDXS spectra corresponding to the recorded TEM images are given in Annex 3. The Cu peaks in these spectra arise from the sample carrier. In the case of cluster **1** anchored and activated onto C_{PPh_2}, the EDXS spectrum shows that the observed particles contain both Ru and Pt. In the case of cluster **2** on C_{PPh_2}, the EDXS spectra indicate that the small and well-dispersed particles are mainly constituted of Ru and that the bigger particles are indeed exclusively constituted of gold. This observation, in addition to the XRD and SIMS results described above, indicates that, for cluster **2**, anchoring on C_{PPh_2} causes its fragmentation

Table 3. Thermogravimetric analyses.

Cluster	Weight loss [%]	Final dec. temp. [°C]	Calcd. weight loss [%]
$[Ru_5PtC(CO)_{14}(COD)]$ (**1**)	38.3	300	41 (= 14CO + 1COD)
$[Ru_6Au_2C(CO)_{16}(PPh_3)_2]$ (**2**)	40.8	720	49 (= 16CO + 2PPh_3)

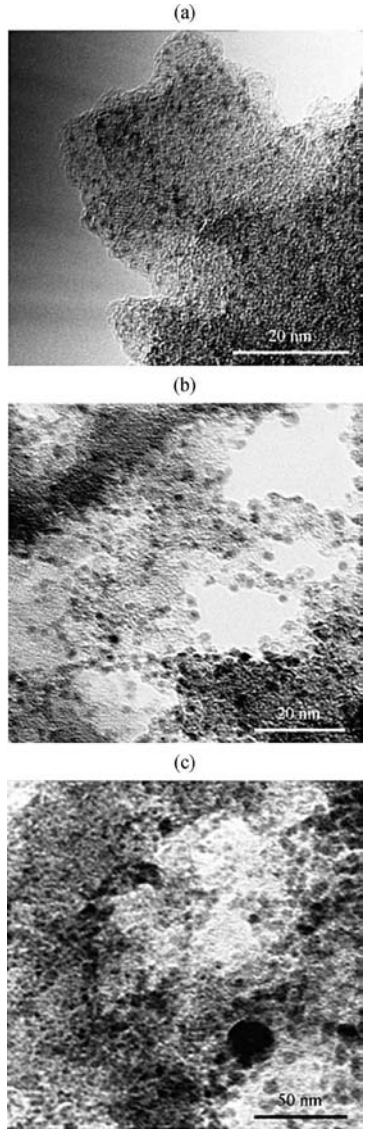

Figure 3. TEM image after thermal treatment: (a) cluster **1** anchored on C_{PPh_2} and (b),(c) cluster **2** supported on C_{PPh_2} (corresponding EDXS spectra are given in Annex 3, see Supporting Information).

and the loss of gold, leading to the formation of homogeneously dispersed Ru-rich nanoparticles together with larger Au particles (Ru-free). This shows that the two clusters behave differently on the same support. In the case of cluster **2**, its interaction with the functionalized support leads to cluster degradation and gold sequestering. Once gold atoms are lost from the grafted cluster, they are prone to agglomeration, giving rise to bigger nanoparticles. Cluster **1** with its readily exchangeable COD ligand was thus more adapted to the grafting strategy developed here. The binding energies (Annex 2, Supporting Information) determined by XPS for each metal in the grafted clusters before activation were close to values corresponding to zero-oxidation states, as expected for organometallic carbonyl clusters, and did not shift much during activation also as expected because it is a mere ligand removal process. Only the gold components shifted by ca. 1 eV during activation for cluster **2**, which is in line with its segregation from the bimetallic starting cluster and its agglomeration into bigger nanoparticles.

2. Model Reaction with $(PPh_2CH_2)_2NC_3H_7$

In order to gain a deeper understanding of the cluster interaction at the surface of C_{PPh_2}, model reactions in solution were carried out. Clusters **1** and **2** were treated with a ligand that mimics as closely as possible the functions present on the C_{PPh_2} surface: namely $(PPh_2CH_2)_2NC_3H_7$. This ligand was successfully synthesized from propylamine, paraformaldehyde and diphenylphosphane (Scheme 3) and its formation was proven by ^1H NMR spectroscopy (Annex 5, Supporting Information): the *a*, *b*, *c*, *d* and *e* hydrogen atoms where observed at 0.76, 1.44, 2.82 and 3.58 ppm, respectively, with correct integrals. The Ph protons were observed between 7.2 and 7.4 ppm. Small quantities of monosubstituted amine ($PPh_2CH_2NHC_3H_7$) were observed as indicated by the additional signals at 0.88, 1.44, 2.69 and 3.38 ppm. The ligand was not isolated as a solid but used directly in solution with the use of cannula techniques.

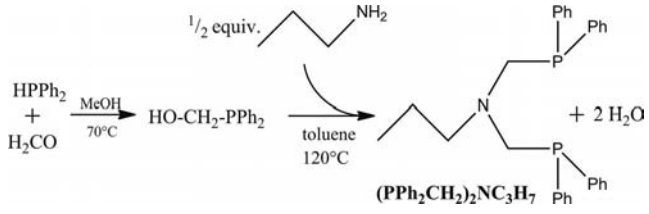

Scheme 3. Synthesis of the ligand used for mimicking the anchoring of clusters **1** and **2** onto C_{PPh_2}.

The $(PPh_2CH_2)_2NC_3H_7$ ligand was first reacted with cluster **1**. The reaction mixture was separated by column chromatography to give three different products. The first product isolated corresponds to the cluster $[Ru_5PtC(CO)_{16}]$ previously described in the literature and very often isolated from reactions involving **1**.[24] The second isolated product displayed CO stretching bands at 2068, 2029 and 2019 cm^{-1}, attributable to terminal carbonyl ligands. The ^1H NMR spectrum indicated only the presence of Ph groups on the cluster, with no signal corresponding to the presence of the C_3H_7 fragment. The single-crystal X-ray diffraction analysis of the obtained monocrystals revealed that this product is the cluster $[Ru_5PtC(CO)_{13}(\mu\text{-}PPh_2)_2]$ (**3**) where phosphides bridge two edges of the Ru_5Pt octahedron (Figure 4). These bridging phosphides have been formed by ligand degradation or from unreacted starting material ($HPPh_2$). This type of product was not fixed on the functionalized carbon surface but was washed out during work-up. Crystallographic data are summarized in Table 4 and selected bond lengths and angles are displayed in Table 5. The distances of the bonds bridged by the μ-PPh_2 groups are shorter than the

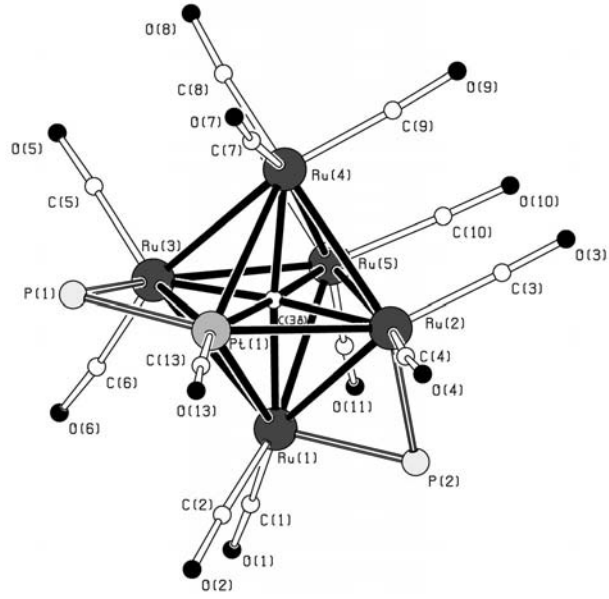

Figure 4. Molecular structure of the cluster $[Ru_5PtC(CO)_{13}(\mu\text{-}PPh_2)_2]$ (**3**) obtained by X-ray crystallography. Ph groups are omitted for clarity.

Table 4. Crystallographic data for $[Ru_5PtC(CO)_{13}(\mu\text{-}PPh_2)_2]$ (**3**) and $[Ru_5PtC(CO)_{14}\{(PPh_2CH_2)_2NC_3H_7\}]\cdot CH_2Cl_2$ (**4**).

	3	**4**
Empirical formula	$C_{38}H_{20}O_{13}P_2Pt_1Ru_5$	$C_{45}H_{33}Cl_2N_1O_{14}P_2Pt_1Ru_5$
M_r [g/mol]	1446.92	1644.99
Temperature [K]	120(2)	120(2)
Crystal system, space group	monoclinic, $P2_1/n$	monoclinic, $P2_1/c$
a [Å]	12.835(3)	9.715(4)
b [Å]	16.647(5)	24.185(9)
c [Å]	19.066(7)	22.134(9)
α [°]	90	90
β [°]	94.21(3)	105.89(3)
γ [°]	90	90
V [Å^3], Z	4063(2), 4	5002(3), 4
Calculated density [g/cm^3]	2.366	2.184
Abs. coefficient [mm^{-1}]	5.385	4.493
θ range [°]	2.92–25.39	2.97–26.37
Reflections collected/ unique/R_{int}	31035/7274/0.060	184735/9576/0.080
Completeness [%]	97.2	93.6
Data/restraints/parameters	7274/0/533	9576/0/633
R_1 [$I > 2\sigma(I)$]	0.0662 [6651]	0.0371 [9528]
Largest resid. peak [e/Å^3]	3.901/–3.578	2.012/–2.478

unbridged ones: 2.7609(12) Å instead of 2.9114(13) Å, 2.9806 Å and 3.0199(14) Å for the Ru–Pt bonds and 2.7774(14) Å instead of 2.9554(14) Å, 2.9416 Å and 2.9344(15) Å for the Ru–Ru bonds of the square plane. This means that the μ-PPh_2 ligands play the same role as CO, shortening metal–metal bonds. The unbridged bonds are in the usual range for Ru–Pt and Ru–Ru bonds of this kind of compound.[19] As far as we know, no other similar species resulting from the addition of bridging phosphides on cluster **1** have been reported so far. Nevertheless, bridging metal-containing moieties have already been added onto a Ru_5Pt cluster to give trimetallic compounds, such as $[Ru_5PtC(CO)_{15}(AuPPh_3)_2]$,[25] $[Ru_5PtC(CO)_{16}(MPtBu_3)_2]$ (M = Pt or Pd)[26] and $[Ru_5PtC(CO)_{16}(MPh_2)_2]$ (M = Ge, Sn or Pb).[27] In these compounds, the bridging fragments are positioned on a Ru–Pt bond or on Ru–Ru bonds of the square plane, as in **3**.

Table 5. Selected bond lengths and angles for cluster **3**.

Distances [Å]		Angles [°]	
Pt(1)–C(13)	1.886(17)	P(1)–Pt(1)–Ru(3)	52.59(8)
Pt(1)–C(38)	2.086(11)	P(1)–Pt(1)–Ru(2)	142.71(8)
Pt(1)–P(1)	2.277(3)	Ru(3)–Pt(1)–Ru(2)	90.58(3)
Pt(1)–Ru(3)	2.7609(12)	P(1)–Pt(1)–Ru(4)	92.61(8)
Pt(1)–Ru(2)	2.9114(13)	Ru(3)–Pt(1)–Ru(4)	61.33(3)
Pt(1)–Ru(4)	2.9806(14)	Ru(2)–Pt(1)–Ru(4)	59.89(3)
Pt(1)–Ru(1)	3.0199(14)	P(1)–Pt(1)–Ru(1)	102.39(9)
Ru(1)–C(1)	1.870(15)	Ru(3)–Pt(1)–Ru(1)	61.30(3)
Ru(1)–C(38)	2.086(12)	Ru(2)–Pt(1)–Ru(1)	55.81(3)
Ru(1)–P(2)	2.280(3)	Ru(4)–Pt(1)–Ru(1)	87.82(3)
Ru(1)–Ru(2)	2.7774(14)	C(38)–Ru(1)–P(2)	99.0(4)
Ru(1)–Ru(5)	2.8950(15)	P(2)–Ru(1)–Ru(2)	52.86(8)
Ru(1)–Ru(3)	2.9554(14)	P(2)–Ru(1)–Ru(5)	90.89(8)
Ru(2)–C(4)	1.896(15)	Ru(2)–Ru(1)–Ru(5)	62.25(3)
Ru(2)–P(2)	2.295(3)	P(2)–Ru(1)–Ru(3)	141.27(8)
Ru(2)–Ru(5)	2.9339(15)	Ru(2)–Ru(1)–Ru(3)	89.35(4)
Ru(2)–Ru(4)	2.9416(15)	Ru(5)–Ru(1)–Ru(3)	59.96(3)
Ru(3)–P(1)	2.274(3)	P(2)–Ru(1)–Pt(1)	103.25(9)
Ru(3)–Ru(5)	2.9237(15)	Ru(5)–Ru(1)–Pt(1)	88.14(3)
Ru(3)–Ru(4)	2.9344(15)	Ru(3)–Ru(1)–Pt(1)	55.03(3)
Ru(4)–C(7)	1.941(17)	P(2)–Ru(2)–Ru(1)	52.38(8)
Ru(4)–Ru(5)	2.8223(16)	P(2)–Ru(2)–Pt(1)	106.22(9)
Ru(5)–C(11)	1.943(16)	Ru(1)–Ru(2)–Pt(1)	64.07(3)
Ru(5)–C(38)	2.030(11)	P(2)–Ru(2)–Ru(5)	89.62(9)
C(1)–O(1)	1.143(17)	Ru(1)–Ru(2)–Ru(5)	60.84(4)
C(2)–O(2)	1.159(18)	Pt(1)–Ru(2)–Ru(5)	89.49(4)
C(3)–O(3)	1.126(17)	P(2)–Ru(2)–Ru(4)	142.82(9)
C(4)–O(4)	1.151(17)	Ru(1)–Ru(2)–Ru(4)	93.34(4)
C(5)–O(5)	1.139(15)	Pt(1)–Ru(2)–Ru(4)	61.22(4)
C(6)–O(6)	1.132(16)	Ru(5)–Ru(2)–Ru(4)	57.42(4)
C(7)–O(7)	1.124(19)	P(1)–Ru(3)–Pt(1)	52.71(8)
C(8)–O(8)	1.140(18)	P(1)–Ru(3)–Ru(5)	144.26(9)
C(9)–O(9)	1.163(18)	Pt(1)–Ru(3)–Ru(5)	92.71(4)
C(10)–O(10)	1.158(17)	P(1)–Ru(3)–Ru(4)	93.91(9)
C(11)–O(11)	1.133(18)	Pt(1)–Ru(3)–Ru(4)	63.03(4)
C(12)–O(12)	1.135(17)	Ru(3)–Ru(4)–Ru(2)	86.67(4)
C(13)–O(13)	1.12(2)	Ru(4)–Ru(5)–Ru(1)	93.41(4)

The third and major product isolated from the reaction between cluster **1** and the ligand $(PPh_2CH_2)_2NC_3H_7$ presented IR stretching bands at 2067, 2043, 2016 and 1968 cm^{-1}. The ^{31}P NMR spectrum showed a singlet at –20 ppm with a ^{195}Pt-^{31}P coupling constant of 4554 Hz, indicating that phosphane groups are linked to the cluster through the Pt atom. The positions and integrals of the peaks in the ^1H NMR spectrum indicate that the whole $(PPh_2CH_2)_2NC_3H_7$ ligand has been added onto the cluster. No signal was found attributable to the COD moiety. These analyses indicate that the $(PPh_2CH_2)_2NC_3H_7$ ligand has reacted with cluster **1** through a ligand exchange mechanism, replacing the COD fragment to be linked by the Pt atom. This was confirmed by the X-ray crystal structure of the product. The obtained crystals corresponded to the cluster $[Ru_5PtC(CO)_{14}\{(PPh_2CH_2)_2NC_3H_7\}]$ (**4**), which crystallized in the $P2_1/c$ space group with a cocrystallized dichloromethane molecule. The crystallographic data are displayed in Table 4 and selected bond lengths and angles of the molecule are displayed in Table 6. The molecular structure of **4** is displayed in Figure 5 showing that the intact $(PPh_2CH_2)_2NC_3H_7$ ligand is linked to the cluster through the Pt atom instead of the COD moiety. The Ru–Pt distances in this structure [2.8779(11) and 3.1366(12) Å] are slightly longer than those of the starting cluster **1** [2.844(2)–3.072(2) Å], even though the Ru–Ru ones are similar [2.8378(10) and 2.9331(12) Å versus 2.826(3)–2.944(4) Å, respectively]. Compound **4** can be compared to cluster $[Ru_5PtC(CO)_{14}(dppe)]$ [dppe = bis(diphenylphos-

Table 6. Selected bond lengths and angles for cluster **4**.

Distances [Å]		Angles [°]	
Pt(1)–C(44)	2.070(5)	C(44)–Pt(1)–P(2)	140.82(14)
Pt(1)–P(2)	2.2822(15)	C(44)–Pt(1)–P(1)	128.73(15)
Pt(1)–P(1)	2.2909(16)	P(2)–Pt(1)–P(1)	89.95(6)
Pt(1)–Ru(2)	2.8779(11)	P(2)–Pt(1)–Ru(2)	97.32(5)
Pt(1)–Ru(1)	2.8981(12)	P(1)–Pt(1)–Ru(2)	171.07(4)
Pt(1)–Ru(4)	3.1012(10)	P(2)–Pt(1)–Ru(1)	132.55(4)
Pt(1)–Ru(3)	3.1366(12)	P(1)–Pt(1)–Ru(1)	112.30(5)
Ru(1)–C(3)	1.907(6)	Ru(2)–Pt(1)–Ru(1)	58.85(3)
Ru(1)–C(44)	2.064(6)	P(2)–Pt(1)–Ru(4)	168.27(4)
Ru(1)–Ru(2)	2.8378(10)	P(1)–Pt(1)–Ru(4)	88.34(4)
Ru(1)–Ru(5)	2.8431(12)	Ru(2)–Pt(1)–Ru(4)	85.57(3)
Ru(1)–Ru(4)	2.9331(12)	Ru(1)–Pt(1)–Ru(4)	58.42(2)
Ru(2)–C(4)	1.887(7)	P(2)–Pt(1)–Ru(3)	117.78(4)
Ru(2)–Ru(5)	2.8430(10)	P(1)–Pt(1)–Ru(3)	123.09(4)
Ru(2)–Ru(3)	2.9072(12)	Ru(2)–Pt(1)–Ru(3)	57.62(3)
Ru(3)–C(7)	1.886(6)	Ru(1)–Pt(1)–Ru(3)	85.31(3)
Ru(3)–C(44)	2.040(5)	Ru(4)–Pt(1)–Ru(3)	54.539(17)
Ru(3)–Ru(5)	2.8188(13)	Ru(2)–Ru(1)–Ru(5)	60.06(2)
Ru(3)–Ru(4)	2.8582(10)	Ru(2)–Ru(1)–Pt(1)	60.22(2)
Ru(4)–C(10)	1.867(6)	Ru(5)–Ru(1)–Ru(4)	58.77(3)
Ru(4)–Ru(5)	2.8354(12)	Pt(1)–Ru(1)–Ru(4)	64.26(3)
P(1)–C(40)	1.853(6)	Ru(1)–Ru(2)–Ru(5)	60.06(3)
P(2)–C(39)	1.854(6)	Ru(1)–Ru(2)–Pt(1)	60.93(2)
C(1)–O(1)	1.145(8)	Ru(1)–Ru(2)–Ru(3)	90.86(3)
C(2)–O(2)	1.136(8)	Ru(5)–Ru(2)–Ru(3)	58.69(2)
C(3)–O(3)	1.150(8)	Pt(1)–Ru(2)–Ru(3)	65.66(3)
C(4)–O(4)	1.147(8)	Ru(5)–Ru(3)–Ru(4)	59.92(2)
C(5)–O(5)	1.132(8)	Ru(5)–Ru(3)–Ru(2)	59.51(3)
C(6)–O(6)	1.152(8)	Ru(4)–Ru(3)–Ru(2)	89.66(3)
C(7)–O(7)	1.143(8)	Ru(5)–Ru(3)–Pt(1)	88.79(4)
C(8)–O(8)	1.155(9)	Ru(4)–Ru(3)–Pt(1)	62.10(2)
C(9)–O(9)	1.132(9)	Ru(2)–Ru(3)–Pt(1)	56.72(3)
C(10)–O(10)	1.156(8)	Ru(5)–Ru(4)–Ru(1)	59.03(3)
C(11)–O(11)	1.133(8)	Ru(1)–Ru(4)–Pt(1)	57.32(2)
C(12)–O(12)	1.157(7)	Ru(3)–Ru(5)–Ru(1)	92.59(4)
C(13)–O(13)	1.138(8)	Ru(4)–Ru(5)–Ru(1)	62.20(3)
C(14)–O(14)	1.135(8)	Ru(2)–Ru(5)–Ru(1)	59.88(2)

phanyl)ethane] obtained by reaction between **1** and dppe.[28] In the latter compound, dppe also replaces the COD ligand and is linked to the cluster by the Pt atom. The Ru–Pt and Ru–Ru distances in this compound are 2.8946(8)–3.1214(8) Å and 2.793(1)–2.949(1) Å, respectively, which is similar to those of cluster **4**. Compound **4** is in agreement with the PSEPT rules, which predict a "closo" octahedron for the metal core. The formation of **4** confirms the ease with which compound **1** exchanges its COD ligand for chelating phosphanes and, thus, confirms the exchange ligand mechanism that could occur at the surface of C_{PPh_2} when clusters are anchored onto it. The fact that the main product isolated from the reaction of the model ligand with cluster **1** is formed by a controlled ligand-exchange process allows us to state that with this cluster it is the main event occurring on the phosphane-functionalized carbon. It is in agreement with the characterization data from the solids and explains why the cluster is poorly dispersed on the nonfunctionalized support, i.e. the nonfunctionalized support does not offer a sufficient anchoring mechanism. The final nanoparticles are very small, demonstrating the ability of the functionalized support to hinder agglomeration during thermal treatment. However, their size is above that of a single cluster core, indicating that some migration and coalescence must occur during heating.

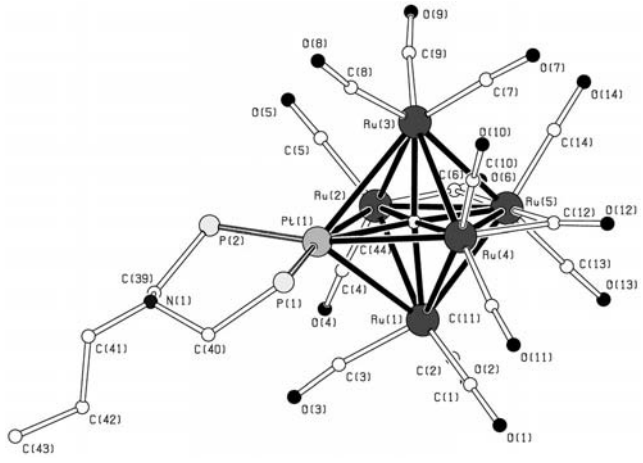

Figure 5. Molecular X-ray structure of the cluster $[Ru_5PtC(CO)_{14}\{(PPh_2CH_2)_2NC_3H_7\}]$ (**4**) obtained by X-ray crystallography; Ph groups are omitted for clarity.

The $(PPh_2CH_2)_2NC_3H_7$ ligand was also reacted with cluster **2**, but led to inconclusive results. Characterization data indicated the presence of different products but only the unreacted starting cluster crystallized out of the complex reaction mixture. This indicates that cluster **2** does not react selectively with chelating phosphane groups, which might be explained by the absence of easily replaced ligands such as COD and the preference of Au for terminal phosphanes. When interacting with the functionalized support this cluster thus undergoes unselective reactions leading to its fragmentation, as evidenced by SIMS. This highlights the powerfulness of this technique to unravel molecular mechanisms within complex solids.

Conclusions

In this work, we have shown that when active carbon is functionalized with chelating phosphane groups mixed-metal clusters can be bound covalently onto its surface. The clusters used have to be sufficiently stable during anchoring to avoid their fragmentation, which would mean losing the advantage of using such precursors. The anchoring of clusters $[Ru_5PtC(CO)_{14}(COD)]$ (COD = cyclooctadiene) (**1**) and $[Ru_6Au_2C(CO)_{16}(PPh_3)_2]$ (**2**) were mimicked in solution and the crystal structure of cluster $[Ru_5PtC(CO)_{14}\{(PPh_2CH_2)_2NC_3H_7\}]$ was the proof of chemical binding of cluster **1** onto C_{PPh_2} through a ligand exchange mechanism. The nanoparticles obtained after thermal activation were better dispersed on C_{PPh_2} than on the unmodified support, proving that the surface functions act as stabilizing sites for the clusters. The use of appropriate mixed-metal clusters and functionalized carbon supports leads to the formation of well-dispersed nanoparticles of controlled composition (corresponding to the stoichiometry of the precursor cluster). We have also shown that a combination of characterization techniques with model reactions in solution enabled us to gain a full picture of the mechanisms occurring at the surface of the solid that is not amenable to simple spectroscopic studies. The obtained nanostructured materials could find applications in electrochemical devices or heterogeneous catalysis.

Experimental Section

General: All manipulations were carried out under N_2 with distilled solvents. $(PPN)_2[Ru_6C(CO)_{16}]$ and $(PPN)_2[Ru_5C(CO)_{14}]$ were synthesized as described previously.[19] $[Pt(COD)Cl_2]$, $[Au(PPh_3)Cl]$ and H_2CO were supplied by Sigma–Aldrich, $H_2NC_3H_7$ by Acros Organics, $HPPh_2$ by Fluka, and all were used as received. The activated carbon SXplus (noted as C_{SX+}) support was supplied by Norit and C_{PPh_2} was prepared as described elsewhere[18,21] and summarized here. The starting carbon (C_{sx+}), with S_{BET} = 932 m^2/g, was oxidized with HNO_3 (2.5 mol/L) to give C_{COOH} (S_{BET} = 701 m^2/g). The oxidized support C_{COOH} was then treated with $SOCl_2$ under nitrogen to give C_{Cl} (S_{BET} = 752 m^2/g), which in turn was treated with ethylenediamine under nitrogen to give C_{NH_2} (S_{BET} = 482 m^2/g) presenting pendant amine groups. Finally, the C_{NH_2} material was treated with $HPPh_2/CH_2O$ under nitrogen for 24 h at 70 °C to give the functionalized support C_{PPh_2} (S_{BET} = 121 m^2/g).

Infrared spectra of the clusters were recorded in a dichloromethane solution with a Bruker Equinox 55 spectrometer. NMR analyses were recorded with an AVANCE 500 or 300 MHz spectrometer. ^1H NMR spectra were calibrated with $CDHCl_2$ at 5.3 ppm and ^{31}P NMR with H_3PO_4 at 0 ppm. Atomic absorption measurements were carried out with a Perkin–Elmer atomic absorption spectrometer 3110. TGA analyses of the clusters were recorded with a TGA SDTA 851e instrument from Mettler–Toledo. These analyses were carried out with a heating ramp of 10 °C/min under a N_2 flow (100 mL/min) and the samples (ca. 3 mg) were placed into alumina containers (70 μL). XPS (X-ray photoelectron spectroscopy) analyses were carried out at room temperature with a SSI-X-probe (SSX-100/206) photoelectron spectrometer from Surface Science Instruments (USA) equipped with a monochromatized microfocus Al X-ray source. Samples were stuck onto small troughs with double-

face adhesive tape and then placed on an insulating home-made ceramic carousel (Macor®, Switzerland). Charge effects were avoided by placing a nickel grid above the samples and using a flood gun set at 8 eV. The energy scale was calibrated with reference to the peak $Au4f_{7/2}$ at 84 eV, and the binding energies were calculated with respect to the *C*-(C,H) component of the C1s peak fixed at 284.8 eV. Data treatment was performed with the CasaXPS program (Casa Software Ltd, UK). The peaks were decomposed into a sum of Gaussian/Lorentzian (85/15) after subtraction of a Shirley type baseline. ToF-SIMS analyses were performed with a PHI-EVANS Time-of-Flight SIMS (TRIFT 1) using a 15 keV Ga^+ beam (FEI 83–2 liquid metal ion source; ca. 1 nA DC current; 22 ns pulse width bunched down to ca. 1 ns; 5 kHz repetition rate for the mass range 0–5 kDa).[29,30] For these analyses all the samples were fixed by silver double-sided conducting adhesive tape onto stainless steel supports. TEM images were obtained with a LEO 922 OMEGA Energy Filter Transmission Electron Microscope. The samples were suspended in hexane under ultrasonic treatment, then allowed to settle to discard the biggest particles. A drop of the supernatant was then deposited on a holey carbon film supported on a copper grid, which was dried overnight under vacuum at room temperature.

Cluster Syntheses: Cluster $[Ru_5PtC(CO)_{14}(COD)]$ (**1**) was obtained in 20.5% yield as described previously[19] from $(PPN)_2[Ru_5C(CO)_{14}]$ and $[Pt(COD)Cl_2]$. IR: $\tilde{\nu}_{CO}$ = 2077 (m), 2050 (s), 2033 (s), 2011 (s), 1987 (sh), 1965 (sh), 1818 (w) cm^{-1}. Cluster $[Ru_6Au_2C(CO)_{16}(PPh_3)_2]$ (**2**) was prepared by reacting $(PPN)_2[Ru_6C(CO)_{16}]$ (100 mg, 0.0466 mmol) with 2 equiv. of $[Au(PPh_3)Cl]$ (46.1 mg; 0.0933 mmol) in dichloromethane (10 mL). The mixture was stirred at room temperature for 1 h, then filtered and the solvent was removed under reduced pressure. The obtained crude product was purified by column chromatography on silica (hexane/dichloromethane, 50:50) to give **2** as a dark-red powder (39.2 mg; 42%). IR: $\tilde{\nu}_{CO}$ = 2068 (w), 2049 (s), 2017 (vs), 1964 (w) and 1820 (m) cm^{-1}. ^1H NMR (500 MHz, CD_2Cl_2, 25 °C, $CDHCl_2$): δ = 7.46–7.57 (m, 6 Ph) ppm. ^{31}P NMR (500 MHz, CD_2Cl_2, 25 °C, H_3PO_4): δ = 67.8 (s, 2 P) ppm.

Anchoring: The amount of cluster engaged in each anchoring experiment corresponded to a theoretical 10 wt.-% metal loading on the support after the removal of the ligand. In a typical experiment, cluster **1** (24.3 mg) was stirred with C_{PPh_2} (126 mg) in toluene (10 mL) and dichloromethane (10 mL) at room temperature for 5 d in the dark. The solid was filtered out, washed with dichloromethane and dried at room temperature under vacuum. The same procedure was used for anchoring cluster **2** onto C_{PPh_2} [using **2** (19.8 mg) and $CPPh_2$ (90 mg)]. Ruthenium atomic absorption analyses of the filtrates indicated that the total metal loading (Ru + Au/Pt) after grafting was 7.8 and 4.2 wt.-% for **1** and **2**, respectively, considering that the stoichiometry of the clusters was not affected by anchoring. Cluster **1** (34.6 mg) was adsorbed onto C_{SX+} (180 mg) in a 2-propanol/dichloromethane (45:5) mixture as described previously[20] and cluster **2** (19.8 mg) was adsorbed similarly onto C_{SX+} (90 mg) in a toluene/dichloromethane (1:1) mixture. In both these cases, the solvents were removed under reduced pressure instead of filtering and 10 wt.-% metal can be considered to have been loaded onto the support. The supported clusters were then submitted to thermal treatment in a tubular oven STF 16/450 from CARBOLITE. The samples were placed into porcelain combustion boats and heated at 300 °C for 1 h for cluster **1** and at 350 °C for 3 h for cluster **2** (heating ramp: 100 °C/h) under a N_2 stream.

Reactions with $(PPh_2CH_2)_2NC_3H_7$: The $(PPh_2CH_2)_2NC_3H_7$ ligand was synthesized by first mixing H_2CO (104.5 mg, 3.481 mmol) with 1 equiv. of $HPPh_2$ (0.60 mL, 3.467 mmol) in methanol (5 mL) for 10 min at 70 °C (formation of $HOCH_2PPh_2$ was indicated by decolouration of the solution). The solution was then cooled to room temperature and the solvent was evaporated under reduced pressure. Subsequently, toluene (10 mL) was added, followed by 0.5 equiv. of $C_3H_7NH_2$ (0.14 mL, 1.703 mmol) and the mixture was heated at 120 °C for 1–2 h. The solution was cooled to room temperature and the volume was reduced to 5 mL. By this method, a toluene solution containing $(PPh_2CH_2)_2NC_3H_7$ (1.703 mmol) was obtained. ^1H NMR (300 MHz, CD_2Cl_2, 25 °C, $CDHCl_2$): δ = 7.2–7.4 (m, 24 H), 3.58 (d, 4 H), 3.38 (d, 0.5 H), 2.82 (t, 2 H), 2.69 (t, 0.5 H), 1.44 (m, 2.75 H), 0.88 (t, 0.8 H) and 0.76 (t, 3 H) ppm. ^{31}P NMR (300 MHz, CD_2Cl_2, 25 °C, H_3PO_4): δ = –26.4 (s) ppm. In the following reactions using the $(PPh_2CH_2)_2NC_3H_7$ ligand, an appropriate quantity of the toluene solution was sampled by means of a syringe.

The anchoring of cluster **1** onto C_{PPh_2} was mimicked in solution by mixing cluster **1** (100 mg, 0.0825 mmol) with 1 equiv. of synthesized $(PPh_2CH_2)_2NC_3H_7$ ligand [0.0851 mmol, 0.25 mL of a toluene solution (5 mL) containing 1.703 mmol of ligand] in dichloromethane (20 mL) for 3 h at room temperature. The solvent was then removed under reduced pressure. The crude product was purified by column chromatography on silica (dichloromethane/hexane, 20:80) to give three different products. The first product to elute, recovered as a red powder, corresponded to the known cluster $[Ru_5PtC(CO)_{16}]$[22] (8.4 mg, 16%). IR: $\tilde{\nu}_{CO}$ = 2064 (s), 2050 (s), 2004 (m) and 1874 (w) cm^{-1}. The second product was isolated as an orange-brown powder and corresponded to the cluster $[Ru_5PtC(CO)_{13}(\mu\text{-}PPh_2)_2]$ (**3**, 9.8 mg, 15%). IR: $\tilde{\nu}_{CO}$ = 2068 (m), 2029 (s) and 2019 (s) cm^{-1}. ^1H NMR (300 MHz, CD_2Cl_2, 25 °C, $CDHCl_2$): δ = 7.3–7.5 (m), 1.52 (s), 1.25 (s) and 0.85 (m) ppm. Suitable crystals for X-ray diffraction were obtained by slow diffusion of hexane into a concentrated solution of **3** in dichloromethane at 4 °C. The last product was isolated as a brown-black powder and identified as the cluster $[Ru_5PtC(CO)_{14}\{(PPh_2CH_2)_2NC_3H_7\}]$ (**4**, 14.8 mg, 20%). IR: $\tilde{\nu}_{CO}$ = 2070 (m), 2043 (s), 2016 (s), 1968 (sh), 1819 (w) and 1714 (w) cm^{-1}. ^{31}P NMR (300 MHz, CD_2Cl_2, 25 °C, H_3PO_4): δ = –19.9 (t, $J_{Pt\text{-}P}$ = 4554 Hz) ppm. ^1H NMR (300 MHz, CD_2Cl_2, 25 °C, $CDHCl_2$): δ = 7.02–8.16 (m, 21 H), 3.53 (t, 4 H), 2.33 (t, 2 H), 1.52 (s, 3 H), 1.19 (m, 5 H) and 0.53 (t, 3 H) ppm. Suitable crystals for X-ray diffraction were obtained by slow diffusion of hexane into a concentrated solution of **4** in dichloromethane at 4 °C.

The anchoring of cluster **2** onto C_{PPh_2} was mimicked in solution by mixing cluster **2** (100 mg, 0.0504 mmol) with 1 equiv. of $(PPh_2CH_2)_2NC_3H_7$ [0.0511 mmol, 0.15 mL of a toluene solution (5 mL) containing 1.7029 mmol of ligand] in dichloromethane (40 mL) for 1 h at room temperature. The solvent was then removed under reduced pressure to give a red powder. IR: $\tilde{\nu}_{CO}$ = 2050 (w) and 2000 (s) cm^{-1}. ^{31}P NMR (300 MHz, CD_2Cl_2, 25 °C, H_3PO_4): δ = 63.77 (s, 1 P), 20.6 (s, 1.7 P) and –9.23 (s, 1 P) ppm. ^1H NMR (300 MHz, CD_2Cl_2, 25 °C, $CDHCl_2$): δ = 7.0–7.5 (m), 3.93 (s), 3.76 (s), 2.49 (t), 2.33 (s), 2.20 (t), 1.26 (m), 0.88 (m), 0.54 (t) and 0.33 (t) ppm. Suitable crystals for X-ray diffraction were obtained by slow diffusion of hexane into a concentrated solution of the crude product in dichloromethane at 4 °C, but the structure obtained corresponded to the starting, unreacted cluster **2**.

Crystal Structure Determination: The X-ray diffraction (XRD) analyses were recorded for the activated clusters with a Siemens D5000 diffractometer equipped with a copper source (λ_{K_α} = 154.18 pm). The samples were placed on quartz monocrystals and the crystalline phases were identified by reference to the JCPDS

database. For single-crystal X-ray diffraction, the X-ray intensity data were collected at 120 K for both clusters with a MAR345 image plate using Mo-K_α (λ = 0.71069 Å) radiation. The crystal was chosen, mounted in inert oil and transferred quickly to the cold gas stream for flash cooling. The crystal data and the data collection parameters are summarized in Table 4. The data were not corrected for absorption but the collection mode partially takes the absorption phenomena into account (see the total number of collected reflections versus the number of independent reflections). The unit cell parameters were refined using all the collected spots after the integration process. Both structures **3** and **4** were solved by the Patterson method and refined by full-matrix least-squares on F^2 using SHELXL97.[31] All the non-hydrogen atoms were refined anisotropically. For both compounds, the hydrogen atoms were calculated with AFIX and included in the refinement with a common isotropic temperature factor. The details of the refinement and the final *R* indices are presented in Table 4.

CCDC-811674 (for **3**) and -811675 (for **4**) contain the supplementary crystallographic data for this paper. These data can be obtained free of charge from The Cambridge Crystallographic Data Centre via www.ccdc.cam.ac.uk/data_request/cif.

Supporting Information (see footnote on the first page of this article): Annex 1: SIMS spectra of C_{PPh_2} after thermal treatment, Annex 2: raw XPS data, Annex 3: EDXS analysis of anchored clusters after thermal treatment, Annex 4: XRD diffractograms and Annex 5: ^{1}H NMR spectrum of $(PPh_2CH_2)_2NC_3H_7$.

Acknowledgments

The authors gratefully acknowledge the Fonds de la Recherche Scientifique (F. N. R. S.), the Fonds pour la Formation à la Recherche dans l'Industrie et dans l'Agriculture (F. R. I. A.) and the Belgian State (Belgian Science Policy, IAP Project INANOMAT N° P6/17) for financial support. NORIT is thanked for supplying the SX+ carbon. P. Lipnik, L. Ryelandt, J.-F. Statsijns, and C. Poleunis are acknowledged for their technical assistance.

[1] B. C. Gates, L. Guzci, H. Knözinger, *Metal Clusters in Catalysis*, *Stud. Surf. Sci. Catal.*, Elsevier Science Publishers, Amsterdam, **1986**, vol. 29.
[2] S. Hermans, R. Raja, J. M. Thomas, B. F. G. Johnson, G. Sankar, D. Gleeson, *Angew. Chem.* **2001**, *113*, 1251; *Angew. Chem. Int. Ed.* **2001**, *40*, 1211.
[3] R. Raja, T. Khimyak, J. M. Thomas, S. Hermans, B. F. G. Johnson, *Angew. Chem.* **2001**, *113*, 4774; *Angew. Chem. Int. Ed.* **2001**, *40*, 4638.
[4] R. Raja, G. Sankar, S. Hermans, D. S. Shephard, S. Bromley, J. M. Thomas, B. F. G. Johnson, *Chem. Commun.* **1999**, 1571.
[5] N. Feeder, J. F. Geng, P. G. Goh, B. F. G. Johnson, C. M. Martin, D. S. Shephard, W. Z. Zhou, *Angew. Chem.* **2000**, *112*, 1727; *Angew. Chem. Int. Ed.* **2000**, *39*, 1661.
[6] C. M. G. Judkins, K. A. Knights, B. F. G. Johnson, Y. R. de Miguel, R. Raja, J. M. Thomas, *Chem. Commun.* **2001**, 2624.
[7] C. Moreno-Castilla, M. A. Salas-Peregrin, F. López-Garzón, *Fuel* **1995**, *74*, 830.
[8] K. Torigoe, H. Remita, G. Picq, J. Belloni, D. Bazin, *J. Phys. Chem. B* **2000**, *104*, 7050.
[9] S. M. Yunusov, E. S. Kalyuzhnaya, H. Mahapatra, V. K. Puri, V. A. Likholobov, V. B. Shur, *J. Mol. Catal. A* **1999**, *139*, 219.
[10] A. R. Silva, M. Martins, M. M. A. Freitas, J. L. Figueiredo, C. Freire, B. de Castro, *Eur. J. Inorg. Chem.* **2004**, 2027.
[11] A. R. Silva, J. L. Figueiredo, C. Freire, B. de Castro, *Catal. Today* **2005**, *102*, 154.
[12] B. Jarrais, A. R. Silva, C. Freire, *Eur. J. Inorg. Chem.* **2005**, 4582.
[13] A. R. Silva, V. Budarin, J. H. Clark, B. de Castro, C. Freire, *Carbon* **2005**, *43*, 2096.
[14] M. S. Nashner, A. I. Frenkel, D. L. Adler, J. R. Shapley, R. G. Nuzzo, *J. Am. Chem. Soc.* **1997**, *119*, 7760.
[15] M. S. Nashner, A. I. Frenkel, D. Somerville, C. W. Hills, J. R. Shapley, R. G. Nuzzo, *J. Am. Chem. Soc.* **1998**, *120*, 8093.
[16] C. W. Hills, M. S. Nashner, A. I. Frenkel, J. R. Shapley, R. G. Nuzzo, *Langmuir* **1999**, *15*, 690.
[17] L.-L. Wang, S. V. Khare, V. Chirita, D. D. Johnson, A. A. Rockett, A. I. Frenkel, N. H. Mack, R. G. Nuzzo, *J. Am. Chem. Soc.* **2006**, *128*, 131.
[18] C. Willocq, S. Hermans, M. Devillers, *J. Phys. Chem. C* **2008**, *112*, 5533.
[19] S. Hermans, T. Khimyak, B. F. G. Johnson, *J. Chem. Soc., Dalton Trans.* **2001**, 3295.
[20] M. I. Bruce, E. Horn, P. A. Humphrey, E. R. T. Tiekink, *J. Organomet. Chem.* **1996**, *518*, 121.
[21] S. Hermans, C. Diverchy, O. Demoulin, V. Dubois, E. M. Gaigneaux, M. Devillers, *J. Catal.* **2006**, *243*, 239.
[22] C. Willocq, A. Delcorte, S. Hermans, P. Bertrand, M. Devillers, *J. Phys. Chem. B* **2005**, *109*, 9482.
[23] S. Hermans, T. Khimyak, N. Feeder, S. J. Teat, B. F. G. Johnson, *Dalton Trans.* **2003**, 672.
[24] R. D. Adams, W. Wu, *J. Cluster Sci.* **1991**, *2*, 271.
[25] T. Khimyak, B. F. G. Johnson, S. Hermans, A. D. Bond, *Dalton Trans.* **2003**, 2651.
[26] R. D. Adams, B. Captain, W. Fu, *J. Organomet. Chem.* **2003**, *682*, 113.
[27] R. D. Adams, B. Captain, W. Fu, *J. Organomet. Chem.* **2003**, *671*, 158.
[28] K. Lee, J. R. Shapley, *Organometallics* **1998**, *17*, 3020.
[29] B. W. Schueler, *Microsc. Microanal. Microstruct.* **1992**, *3*, 119.
[30] A. Delcorte, X. Vanden Eynde, P. Bertrand, D. F. Reich, *Int. J. Mass Spectrom.* **1999**, *189*, 133.
[31] G. M. Sheldrick, *SHELXS* and *SHELXL-97*, *Programs for Crystal Structure Solution and Refinement*, University of Göttingen, Germany, **1997**.

Received: April 8, 2011
Published Online: September 7, 2011

